Scientific Journal for Damietta Faculty of Science **15**(2) 2025, 1-10
Doi: 10.21608/sjdfs.2025.402163.1243
ISSN Print 2314-8594
ISSN Online 2314-8616

https://sjdfs.journals.ekb.eg/

Chaos Suppression in an Electrodynamic Tethered Satellite System via Sliding Mode Control under J_2 Perturbation

A. Yousof*[1], A.M. Abdelaziz[2], Abd El Hakeem Abd El Naby[1] and Yehia A. Abdel-Aziz[2]

[1]Damietta University, Mathematics Department, Damietta, Egypt.
[2]National Research Institute of Astronomy and Geophysics (NRIAG), Cairo, Egypt.

Received: 09 July 2025 /Accepted: 20 July 2025

*Corresponding author's E-mail: A.usf@du.edu.eg

Abstract

This paper investigates the chaotic dynamics of an in-plane electrodynamic tethered satellite system (EDTSS) influenced by Earth's oblateness. The system is modelled using the dumbbell model, and the equations of motion are derived via the Lagrangian approach, accounting for the Lorentz force and the perturbation caused by the J_2 zonal harmonic. The onset of chaos is analytically examined using Melnikov's method, which provides a necessary condition for the emergence of chaotic behavior in the system. To address this instability, a novel control strategy based on sliding mode control (SMC) is proposed, with the tether length serving as the control input. The controller is designed to suppress chaotic motion and guide the system toward either a desired oscillatory behavior or a predefined equilibrium point. Numerical simulations are carried out to verify the analytical condition for chaos and to evaluate the effectiveness of the proposed SMC-based tether length control. The results confirm the controller's capability to stabilize the system and eliminate undesired chaotic responses.

Keywords: Chaos, Earth's oblateness, Electromagnetic Force, Melnikov Analysis, Sliding Mode Control, Tethered Satellite System.

Introduction

Space debris represents one of the most pressing challenges facing the global space community today. It is defined as all man-made objects in orbit or re-entering the Earth's atmosphere including defunct satellites, spent rocket stages, and fragments from disintegration, erosion, and collisions that no longer serve any useful function, Unoosa (2010). As of 05 May 2025, the European Space Agency (ESA), using the MASTER-8 model, estimates that approximately 54,000 objects larger than 10 cm are currently orbiting Earth, including around 9,300 active payloads. In addition, nearly 1.2 million debris fragments range in size from 1 cm to 10 cm, while an estimated 140 million fragments measure between 1 mm and 1 cm. To address this growing threat, researchers and engineers have been actively developing

innovative technologies for debris mitigation and removal. Among these, electrodynamic tethered satellite systems have emerged as a promising solution for enabling highly efficient and cost-effective space operations.(Ma X and Wen H (2023); Razzaghi P et al. (2021); Svotina V and Cherkasova M (2023))

As a result, the tethered satellite system (TSS) has become one of the most prominent and actively explored topics in space science research (Modi V et al. (1990); Kumar K (2006); Sanmartin JR et al. (2010); Huang P et al. (2018); Sánchez-Arriaga G et al. (2024)).

A typical TSS consists of two or more satellites connected by a tether. Extensive research has been dedicated to the modelling, dynamic analysis, and control of such systems (Hong AaT et al. (2024); Andrievsky B et al. (2022)). To derive the equations of motion, both Newtonian and Lagrangian mechanics are commonly employed, and the system states are usually described using either orbital elements or libration angles. The tether itself is modelled in different forms either as massless or with mass, and either rigid or flexible depending on the specific objectives and assumptions of each study (Aslanov V and Ledkov A (2012); Troger H et al. (2010)).

The dynamics of tethered satellite missions are highly sensitive to various environmental disturbances, which must be carefully addressed during the modelling and control design phases. Key perturbative forces include aerodynamic drag, particularly significant in low Earth orbit, solar radiation pressure, which exerts continuous but subtle variations in force, and Earth's oblateness, characterized by the J_2 zonal harmonic, which distorts the gravitational field and influences orbital stability. Additionally, other disturbances such as third-body gravitational effects and magnetic torques may also affect the system, depending on the specific mission parameters. Properly accounting for these perturbations is critical for accurately predicting system behavior and ensuring the effectiveness and long-term reliability of tethered satellite operations.

Due to the significant influence of Earth's oblateness which is represented by the J_2 coefficient, numerous studies have investigated its effects on the dynamics of orbital and tethered satellite systems. Zheng P et al. (2008) developed a mathematical model using Lagrangian mechanics and performed numerical simulations to analyze the deployment of a tether-assisted deorbit system under the influence of J_2 perturbation. Their findings revealed that the J_2 effect predominantly influences in-plane motion during deployment, without causing out-of-plane motion when the initial out-of-plane angle is zero. Yu B and Jin D (2010) examined a viscoelastic tethered satellite system, assessing the combined effects of J_2 and thermal perturbations. Their results showed that J_2 has a notable impact on deployment—especially in the presence of friction—while thermal perturbations mainly affect retrieval, leading to distinct motion profiles. In a subsequent study, Yu B et al. (2016) extended the analysis to a flexible tethered satellite system subjected to additional disturbances, including atmospheric drag, solar radiation pressure, and orbital eccentricity. Using a simplified two-degree-of-freedom model, their simulations revealed the emergence of bifurcations, quasi-periodic oscillations, and chaotic dynamics. They concluded that J_2 and thermal effects significantly affect pitch motion and must be considered in system design, whereas the impact of drag and solar pressure depends on orbital altitude. Later, Yu B et al. (2020) employed Melnikov analysis to identify conditions under which chaos emerges in a tethered satellite system in a circular orbit. Their study showed that the combined influence of J_2 and aerodynamic drag could trigger chaotic motion even in systems with rigid tethers. Yuan W et al. (2024) further investigated the chaotic dynamics of a tether-sail system in polar orbits, demonstrating through Lagrangian modelling and Melnikov analysis that both J_2 perturbation and orbital eccentricity contribute to enhanced chaotic behavior.

Electrodynamic tethers (EDTs) offer significant advantages over traditional tether systems by enabling propellant-free generation of Lorentz forces, which can be harnessed for efficient orbit control and power generation. Several studies have explored the influence of Earth's J_2 perturbation on the dynamics and control of EDT systems. Hallaj MaA and Assadian N (2016) modelled a tethered satellite formation as a massless rigid dumbbell system subjected to both electrodynamic forces and J_2 perturbation. Their results demonstrated that precise and fuel-free formation control is achievable using electromagnetic actuation in combination with sliding mode control.

Tikhonov A et al. (2017) investigated an electrodynamic control system's ability to counteract gravity gradient torques induced by the J_2 effect in near-Earth orbits, confirming its effectiveness in stabilizing satellite attitude. Razzaghi P et al. (2019) developed a viscoelastic tether model for space debris deorbiting, incorporating both J_2 perturbation and atmospheric drag. They compared the performance of sliding mode control (SMC) and state-dependent Riccati equation (SDRE) controllers, finding that while both approaches stabilized librational motion and reduced orbital altitude, SMC achieved faster responses and exhibited greater robustness to system uncertainties. More recently, Liu J et al. (2021) proposed a fuzzy logic controller for managing continuous current flow in an EDT system under the influence of J_2 and drag forces. Their approach outperformed traditional on-off control strategies by improving orbital boost efficiency and enhancing libration suppression across a range of orbital inclinations.

In this paper, a control strategy based on sliding mode control is proposed to supress the chaotic motion of the system, either by guiding it toward a desired periodic trajectory or stabilizing it at a predefined equilibrium state. The structure of the paper is as follows: Section 2 presents the system modelling, where a dumbbell representation with a non-negligible tether mass is adopted, and the equations of motion are derived using the Lagrangian method. Section 3 applies the analytical Melnikov technique to determine the conditions under which chaotic motion may arise. In Section 4, a sliding mode controller is developed to mitigate chaotic behavior by adjusting the tether length. Section 5 provides numerical simulations that confirm the analytical findings and illustrate the performance of the proposed control scheme. Finally, Section 6 offers concluding remarks.

Mathematical Model

A tethered satellite system (TSS) in a circular orbit around Earth is considered, as depicted in Fig. 1. The system is represented by a dumbbell model, comprising a mother satellite connected to a subsatellite through a tether. The corresponding masses of the mother satellite, subsatellite, and tether are denoted by m_1, m_2, and m_t, respectively.

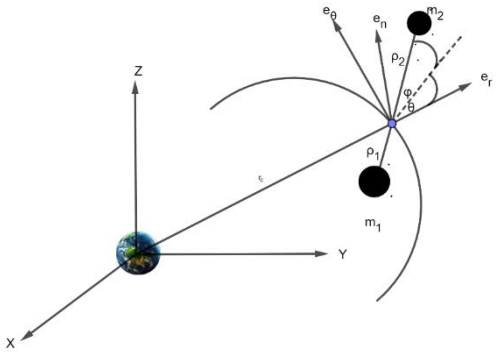

Fig. 1 Tethered Satellite System

An inertial coordinate frame (X, Y, Z), is defined with its origin at the center of the Earth. The X -axis points toward the vernal equinox, the Z -axis is aligned with Earth's rotational axis, and the Y -axis lies in the equatorial plane, forming a right-handed coordinate system.

A rotating reference frame, (e_r, e_θ, e_n), centered at the system's center of mass, is defined with a relative position vector $\boldsymbol{r}_c$ with respect to the inertial frame. The three unit vectors (e_r, e_θ, e_n) point radially outward away from Earth's center of mass, align with the direction of velocity, and complete a right-handed coordinate system, respectively.

The position vectors of the mother satellite and the subsatellite relative to the system's center of mass are denoted by $\boldsymbol{\rho_1}$ and $\boldsymbol{\rho_2}$, respectively. The variable θ represents the in-plane angle, while l indicates the tether length at any given time.

To construct the system's Lagrangian, appropriate expressions for both kinetic and potential energies are required. The total kinetic energy T, can be obtained by integrating the kinetic energy along the tether and summing it with the kinetic energies of the mother satellite and the subsatellite, as described by Aslanov V and Ledkov A (2012).

$$T = \frac{1}{2} m \dot{\boldsymbol{r}}_c . \dot{\boldsymbol{r}}_c + \frac{1}{2} \mu_e (\dot{l}^2 + l^2 (\dot{\theta} + \dot{\nu})^2, \qquad (1)$$

where $m = m_1 + m_2 + m_t$ is a total mass, the dot represents the derivative with respect to time, $\mu_e = (m_1 + m_t / 2)(m_2 + m_t / 2) / (m_1 + m_2 + m_t) - m_t / 6$ is a reduced mass, and ν is the true anomaly.

By summing the potential energies of all system components, and by considering that the tether length is negligible compared to the distance from the system's mass center to Earth, the total potential energy of the system, W, can be

expressed as follows:

$$W = -\frac{\mu m}{r_C} - \frac{\mu \mu_e l^2}{2r_C^3}\left(3\cos^2\theta - 1\right), \quad (2)$$

where μ is Earth's gravitational strength constant.

Based on Eqs. (1) and (2), the Lagrangian, $\mathcal{L}$, is formulated as the difference between the total kinetic and potential energies, i.e., $\mathcal{L} = T - W$. The corresponding equations of motion derived from the Lagrangian take the following form:

$$\frac{d}{dt}\frac{\partial \mathcal{L}}{\partial \dot{q}_i} - \frac{\partial \mathcal{L}}{\partial q_i} = Q_i, \quad (3)$$

here, the generalized coordinates are $q_i = \theta, l$ and Q_i represent non-conservative generalized forces.

By applying the following nondimensional transformation:

$$\frac{d(\,)}{dt} = \frac{d(\,)}{d\nu}\dot{\nu}, L = \frac{l}{l_r},$$

the equations of motion can be reformulated in nondimensional form as follows:

$$\theta'' + 2(\theta' + 1)\frac{L'}{L} + 3\cos\theta\sin\theta = \frac{Q_\theta}{\mu_e l^2 \dot{\nu}^2}, \quad (4)$$

$$L'' - L\left[(\theta' + 1)^2 - 3\cos^2\theta + 1\right] = \frac{Q_l}{\mu_e \dot{\nu}^2}, \quad (5)$$

here, the prime symbol denotes differentiation with respect to the variable ν and $\dot{\nu}^2 = \mu / r_c^3$.

The system is influenced by the Lorentz force generated from the interaction between the electric current flowing through the tether and the surrounding magnetic field, along with the J_2 perturbation caused by Earth's oblateness. A non-tilted dipole model is used to represent the magnetic field, and its components in the orbital frame B_r, B_θ, and B_n, are defined as follows Stevens RE (2008):

$$B_r = -2\frac{\mu_m}{r_c^3}\sin\nu\sin i, \quad (6)$$

$$B_\theta = \frac{\mu_m}{r_c^3}\cos\nu\sin i, \quad (7)$$

$$B_n = \frac{\mu_m}{r_c^3}\cos i, \quad (8)$$

here, i represents the orbital inclination, and $\mu_m = 7.85\,10^{15}\ N/Am^2$, denotes the magnetic dipole moment of Earth. It is assumed that a constant current I, flows along the tether, and the magnetic field remains uniform along its length. This assumption is justified by the relatively short tether length compared to the characteristic radius of the system. According to the principle of virtual work, the generalized electromagnetic torques $Q_{\theta e}$, and Q_{le}, can be expressed as:

$$Q_{\theta,e} = -\frac{Il^2(m_2 - m_1)}{2\left(m_1 + m_2 + m_t\right)}B_n, \quad (9)$$

$$Q_{l,e} = 0.$$

The influence of Earth's oblateness on the dynamics of the tethered satellite system can be assessed through its non-uniform gravitational potential, denoted by U, as described by Kéchichian JA (2021). This potential is given by:

$$U = \frac{\mu}{r_c}\left[1 - \sum_{n=2}^{\infty} J_n \left(\frac{R}{r_c}\right)^n P_n(\sin(\delta))\right], \quad (10)$$

where J_n represents the zonal harmonic coefficient of order n, R is Earth's equatorial radius, and δ is the declination of the system's center of mass relative to the equatorial plane. The term $P_n(\sin(\delta))$ denotes the Legendre polynomial of degree n evaluated at $\sin(\delta)$. By disregarding higher-order terms such as J_3 and above, substituting $\sin(\delta)$ with z / r_c, and applying the transformation matrix to the rotating reference frame, the radial component of the perturbation acceleration can be derived as:

$$\boldsymbol{a}_{ob} = -\frac{3}{2}\frac{J_2 \mu R^2 \boldsymbol{r}_c}{r_c^5}\left(1 - 3\sin^2 i \sin^2 \nu\right). \quad (11)$$

According to Zhong R and Zhu Z (2013), the torque acting on the satellites due to Earth's oblateness-induced acceleration can be expressed as:

$$Q_{\theta,ob} = \gamma\sin(\theta) + \beta\sin(\theta)\cos(2\nu), \quad (12)$$

where

$$\gamma = \chi.\left(1 - \frac{3\sin^2 i}{2}\right), \beta = \chi.\left(\frac{3\sin^2 i}{2}\right),$$

$$\chi = \left(\frac{3J_2 \mu R^2 l^2\left[m_2 M_m^2 - m_1\left(1 - M_m\right)^2\right]}{2r_c^5}\right), \quad (13)$$

where $M_m = (m_1 + m_t / 2) / m$.

In this study, we focus on analysing the nonlinear behavior of pitch motion during the station-keeping phase, where the tether length is held constant. By substituting Eqs. (9), (12) into Eq. (4), assuming $L' = 0$, and considering that

the total torque Q_θ is the sum of the electromagnetic and oblateness contributions, i.e., $Q_\theta = Q_{\theta,e} + Q_{\theta,ob}$, we obtain:

$$\theta'' + 3\cos\theta\sin\theta = \sigma_1 \sin\theta + \sigma_2 \sin\theta\cos 2\nu + \sigma_3, \quad (14)$$

where

$$\sigma_1 = \sigma^*.\left(1 - \frac{3\sin^2 i}{2}\right), \sigma_2 = \sigma^*.\left(\frac{3\sin^2 i}{2}\right),$$

$$\sigma^* = \left(\frac{3J_2R^2\left[m_2M_m^2 - m_1\left(1-M_m\right)^2\right]}{2\mu_e r_c^2}\right), \quad (15)$$

$$\sigma_3 = -\frac{I(m_2 - m_1)\mu_m \cos i}{2m\mu_e\mu}.$$

It is evident from Eq. (14) that the electrodynamic tethered satellite system, when influenced by Earth's oblateness, exhibits the characteristics of a nonlinear and nonautonomous system.

1 Analysis of Chaotic Motion

In this section, the Melnikov method is utilized to establish the necessary condition under which chaotic behaviour may appear in the dynamics of the system.

By defining the state vector as $\boldsymbol{\theta} = \left(\theta_1, \theta_2\right)^T = \left(\theta, \dot{\theta}\right)^T$, the state-space representation of Eq. (14) can be written as:

$$\boldsymbol{\theta} = \boldsymbol{f}\left(\boldsymbol{\theta}\right) + \boldsymbol{g}\left(\boldsymbol{\theta}, \nu\right), \quad (16)$$

where

$$\mathbf{f}(\boldsymbol{\theta}) = \begin{bmatrix} f_1 \\ f_2 \end{bmatrix} = \begin{bmatrix} \theta_2 \\ -3\sin\theta_1\cos\theta_1 \end{bmatrix}, \quad (17)$$

$$\mathbf{g}(\boldsymbol{\theta}, \nu) = \begin{bmatrix} g_1 \\ g_2 \end{bmatrix} = \begin{bmatrix} 0 \\ \sigma_1\sin\theta_1 + \sigma_2\sin\theta_1\cos 2\nu + \sigma_3 \end{bmatrix}. \quad (18)$$

The perturbation vector, $\mathbf{g}(\boldsymbol{\theta}, \nu) = \mathbf{g}(\boldsymbol{\theta}, \nu + p)$, is periodic of period $p = \pi$.

When $\mathbf{g}(\boldsymbol{\theta}, \nu) = 0$, the system reduces to the unperturbed Hamiltonian form. In this case, the first integral of motion is expressed as:

$$\frac{1}{2}\theta_2^{\,2} + \frac{3}{2}\sin^2\theta_1 = E, \quad (19)$$

where E is a constant that denotes the total kinetic energy of the system.

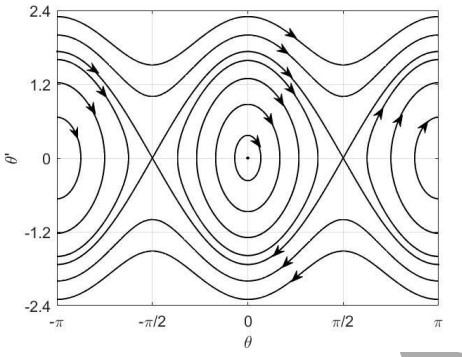

Fig. 2 Phase portrait of unperturbed system

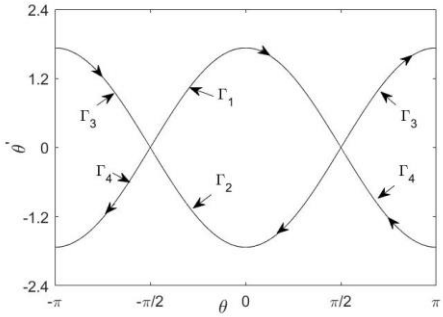

Fig. 3 Heteroclinic orbits

Fig. 2 and Fig. 3 illustrate the phase portrait of the unperturbed system, along with the heteroclinic orbits that connect two distinct saddle points given by $p_i = (\mp\pi/2, 0), i = 1, 2$. The analytical expressions for these heteroclinic orbits are provided in Yu B et al. (2020)

$$\left(\theta_{10}^{\pm}(\nu), \theta_{20}^{\pm}(\nu)\right) = \left(\pm\sin^{-1}(\tanh(\sqrt{3}\nu)), \pm\sqrt{3}\,\mathrm{sech}(\sqrt{3}\nu)\right). \quad (20)$$

For the perturbed system, when $\mathbf{g}(\boldsymbol{\theta}, \nu) \neq 0$, near the equilibrium points, the heteroclinic orbits may divide into unstable and stable manifolds. Chaotic behavior is likely to occur if these manifolds intersect transversely. Based on Melnikov's theory, such a transverse intersection takes place when the Melnikov function has a simple zero (Yu B et al. (2022); Aslanov V (2017)).

The Melnikov function is defined as stated by Aslanov VS (2024)

$$M_{\pm}(\nu_0) = \int_{-\infty}^{+\infty} \boldsymbol{f}\left(\theta_0^{\pm}\right) \wedge \boldsymbol{g}\left(\theta_0^{\pm}, \nu + \nu_0\right) d\nu, \quad (21)$$

with $\nu_0 \in [0, p]$.

By substituting the expressions from Eq. (17) and Eq. (18) into Eq. (21) and performing the necessary integration steps, the resulting

expression for $M_{\pm}(\nu_0)$ reveals terms involving products of even and odd functions over symmetric intervals. Notably, the integrals of odd functions over symmetric bounds cancel out, yielding zero. Based on this analysis and under the condition $\sin 2\nu_0 \in [-1,1]$, the Melnikov function possesses simple zeros if the following inequality holds:

$$\left|\frac{\sigma_3}{\sigma_2}\right| < 0.2881. \tag{22}$$

This condition, though necessary, is not sufficient on its own to guarantee chaos. It indicates that the system may exhibit chaotic dynamics near the saddle points when satisfied.

Tether Length Control

In this section, the sliding mode control method is applied to suppress the chaotic motion observed in the electrodynamic tethered satellite system by designing a controller that acts through tether length modulation.

With the state vector defined as $\boldsymbol{\theta} = (\theta_1, \theta_2)^T = (\theta, \theta')^T$, using Eq. (9) and Eq. (12), Eq. (4) can be rewritten in the state-space form

$$\begin{aligned} \theta_1' &= \theta_2, \\ \theta_2' &= \sigma_1 \sin\theta + \sigma_2 \sin\theta\cos 2\nu + \sigma_3 \\ &\quad -2(\theta_2+1)u - 3\cos\theta\sin\theta, \end{aligned} \tag{23}$$

where $u = L'/L$ represents the control input, which can be adjusted by actuating the reel mechanism on the mother satellite.

The sliding surface for the controlled system is defined by

$$s = \boldsymbol{A}\boldsymbol{e}_{err}^T \tag{24}$$

where $\boldsymbol{A} = [a_1, a_2]$ is a constant vector with $a_2 = 1$ and $a_1 > 0$, (Hurwitz condition).

The tracking error state vector is defined as:

$$\boldsymbol{e}_{err}^T = \begin{bmatrix} e_{err} \\ e'_{err} \end{bmatrix} = \begin{bmatrix} e_1 \\ e_2 \end{bmatrix} = \begin{bmatrix} \theta_1 - \theta_{1d} \\ \theta_2 - \theta_{2d} \end{bmatrix} \tag{25}$$

where θ_{1d} and θ_{2d} denote the desired states or trajectories, depending on the control objective.

To proceed with controller design, the derivative of the sliding surface is computed as follows

$$\begin{aligned} s' &= a_1 e'_1 + e'_2 \\ &= a_1(\theta_1' - \theta_{1d}') + (\theta_2' - \theta_{2d}') \\ &= a_1(\theta_1' - \theta_{1d}') + F(\boldsymbol{\theta}, \nu) - 2(\theta_2+1)u - \theta_{2d}', \end{aligned} \tag{26}$$

where

$$F(\boldsymbol{\theta}, \nu) = \sigma_1 \sin\theta + \sigma_2 \sin\theta\cos 2\nu + \sigma_3 - 3\cos\theta\sin\theta.$$

By using the constant rate reaching law $s' = -k\,\mathrm{sign}(s), k > 0$, and substituting into Eq. (26), the control input u can be obtained as

$$\begin{aligned} u = \frac{1}{2(\theta_2+1)}\big[& a_1(\theta_1' - \theta_{1d}') + F(\boldsymbol{\theta}, \nu) - \theta_{2d}' \\ & + k\,\mathrm{sign}(s)\big]. \end{aligned} \tag{27}$$

The selection of the gain k is a critical aspect of controller design. As noted in Liu J (2017), a small value of k can result in an excessively long reaching time, thereby diminishing the controller's effectiveness. Conversely, a large value may induce chattering, which is undesirable in practical implementations.

To verify the stability of the controlled system, a positive definite Lyapunov function is selected as $V = \frac{1}{2}s^2$. Taking its derivative yields:

$$\begin{aligned} V' &= s\,s' \\ &= s(-k\,\mathrm{sign}(s)) = -k\,|s| < 0. \end{aligned} \tag{28}$$

From Eq. (28), it is evident that the Lyapunov function is negative definite. Hence, the controlled system described in Eq. (23) is asymptotically stable.

Numerical Results

This section presents numerical simulations to verify the necessary condition for the onset of chaotic motion, as given by Eq. (22). This condition indicates that for certain values of σ_3 (representing the Lorentz effect) and σ_2 (representing the oblateness effect), the system may exhibit chaotic behavior if the condition is satisfied. In addition to validating this analytical condition, the effectiveness of the proposed sliding mode controller based on tether length control is also evaluated for its ability to guide the system toward either a desired state or a desired trajectory.

The system parameters used in the simulation are as follows. The mother satellite mass, $m_1 = 1020\,Kg$, the subsatellite mass, $m_2 = 70\,Kg$, and the tether mass, $m_t = 3.4\,Kg$. The system is assumed to orbit the Earth in a circular orbit at an altitude of $600\,Km$, and an inclination of 63°.

The initial conditions of the system are given by $(\theta,\theta') = (-\pi/2 + \pi/100, 0)$, where $\pi/100$ represents a small perturbation angle that places the system close to the unstable saddle point at $(\mp\pi/2, 0)$.

It can be observed that σ_2 and σ_3 are functions of the electric current I flowing through the tether, the orbital inclination i ,and the orbital altitude H.

For a system orbit with an inclination of $\pi/6$, a current of 1 mA flowing through the tether, and an altitude of 600 km, the necessary condition provided by Eq. (22) is satisfied, indicating that the system may exhibit chaotic behavior.

Fig. 4 confirms the presence of chaotic behavior in the system, as the Poincaré section displays discrete points clustered near the saddle point. Fig. 5 illustrates that the pitch angle exhibits irregular oscillations, further confirming the chaotic behavior of the system.

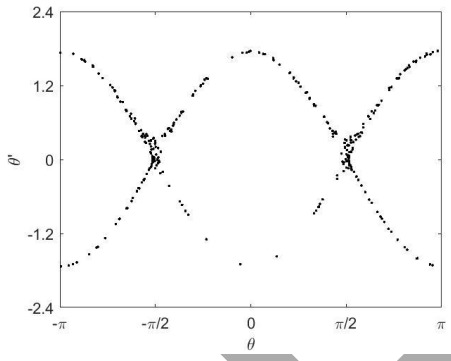

Fig. 4 Poincaré section

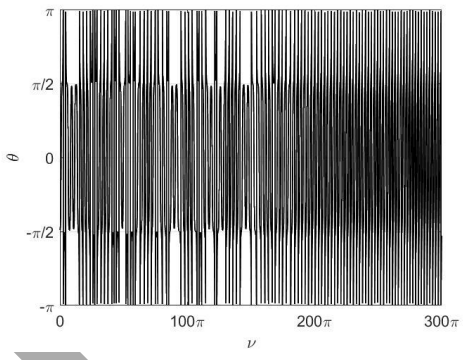

Fig. 5 Pitch angle versus ν

When the system's inclination is $\pi/60$, and a current of 1 mA flows through the tether at an altitude of 900 km, the necessary condition given by Eq. (22) is satisfied. The Poincaré section shown in Fig. 6, corresponding to this state, indicates that the system exhibits chaotic motion. Additionally, Fig. 7 shows that the pitch angle behaves as an irregular oscillator, further confirming the presence of chaos.

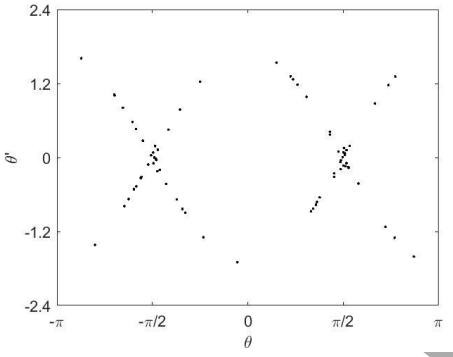

Fig. 6 Poincaré section

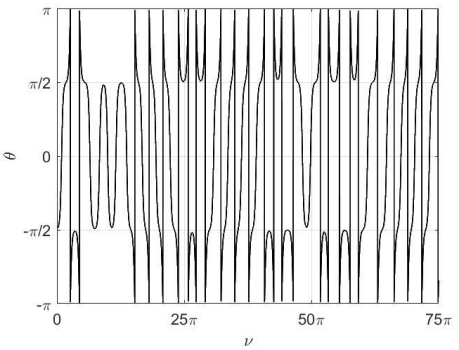

Fig. 7 Pitch angle versus ν

Another case is considered when the system has an inclination of $\pi/30$, with a current of 0.3×10^{-4} (A) flowing through the tether at an altitude of 600 km. In this scenario, the necessary condition given by Eq. (22) is also satisfied. Fig. 8 and Fig. 9 confirm this result, demonstrating that the system exhibits chaotic behavior.

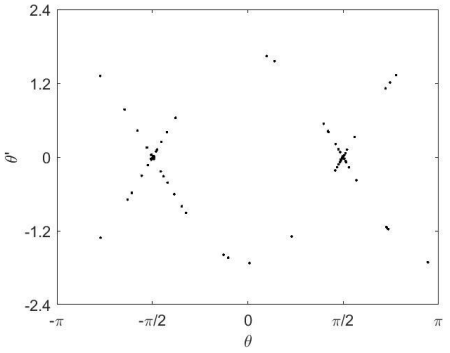

Fig. 8 Poincaré section

The following numerical simulations evaluate the effectiveness of tether length control using a sliding mode controller. This controller is designed to suppress the chaotic motion illustrated in Fig. 4 and Fig. 5, allowing the system to either follow a desired oscillatory behavior or steer the chaotic motion toward a predefined pitch angle through the proposed

control law.

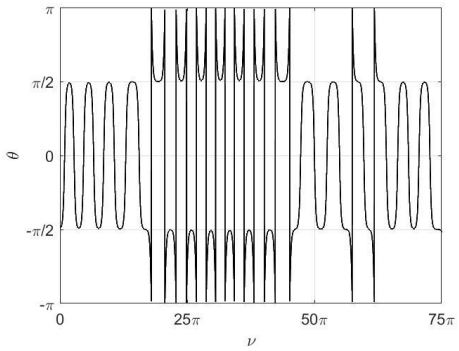

Fig. 9 Pitch angle versus υ

Fig. 10 and Error! Reference source not found. demonstrate the controller's ability to stabilize the system into a desired oscillatory state. As illustrated, the controlled system exhibits periodic behavior similar to that of the unperturbed system, with a period of 11.2155. Fig. 12 and

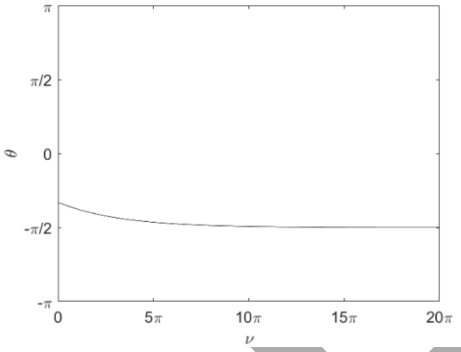

Fig. 13 demonstrate that the controller effectively drives the chaotic motion toward the desired equilibrium point from the initial condition $(-\pi/3, 0)$.

Fig. 12 presents the Poincaré section, which clearly illustrates the system's convergence toward the desired equilibrium point. This is further supported by

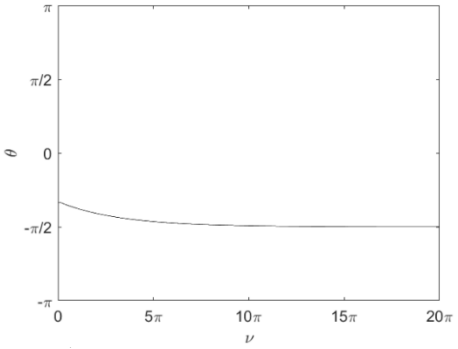

Fig. 13, which shows the variation of the pitch angle with respect to the true anomaly, confirming the system's tendency to settle at the target equilibrium.

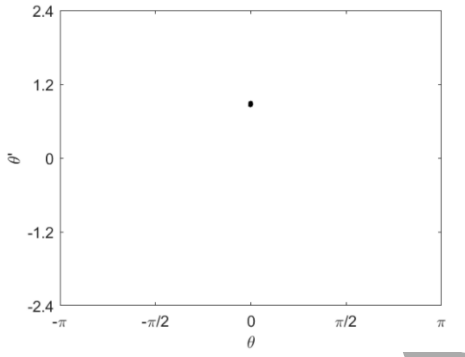

Fig. 10 Poincaré section

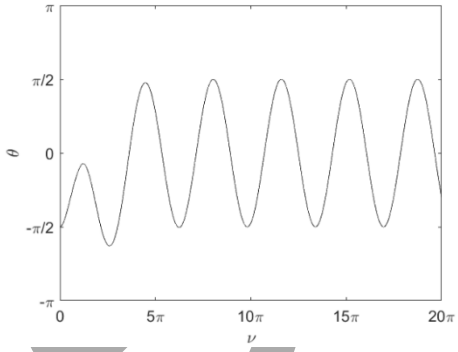

Fig. 11 Pitch angle versus υ

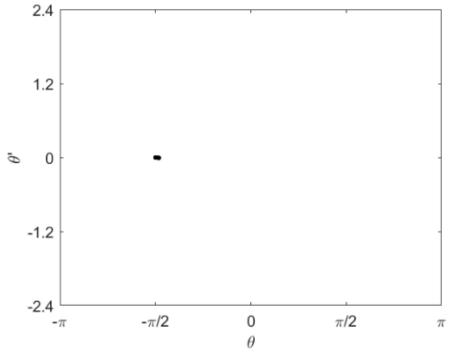

Fig. 12 Poincaré section

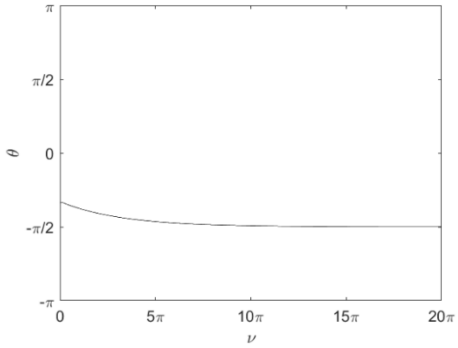

Fig. 13 Pitch angle versus υ

Conclusions

This study presented a control strategy based on sliding mode control (SMC) to regulate the pitch motion of an electrodynamic tethered satellite system (EDTSS) in a circular orbit around Earth. The system was modelled using a dumbbell configuration, taking into account perturbations from both the Lorentz force, generated by the interaction between the current flowing through the tether and Earth's magnetic field, and the Earth's oblateness (J_2 effect). The equations of motion were derived using the Lagrangian approach.

Melnikov analysis was applied to determine the necessary condition under which the system may exhibit chaotic behavior. Numerical simulations were conducted to validate the analytical findings and to demonstrate the existence of chaos under certain conditions. Furthermore, the effectiveness of the proposed SMC-based controller, which utilizes tether length as the control input, was verified. The controller successfully suppressed chaotic motion and steered the system either toward a desired periodic trajectory or a predefined equilibrium point.

The results confirm the robustness and efficiency of the proposed control strategy in stabilizing the chaotic behavior of the EDTSS. However, further experimental validation is recommended to support the theoretical and numerical findings. This research offers valuable insights into the dynamic behavior and control of tethered satellite systems and contributes to the development of reliable methods for their real-world implementation

References

Unoosa. (2010). Space debris mitigation guidelines of the committee on the peaceful uses of outer space.

Ma X, and Wen H (2023) Deep learning for deorbiting control of an electrodynamic tether system. Acta Astronautica. 202: 26-33. https://doi.org/10.1016/j.actaastro.2022.10.019.

Razzaghi P, Al Khatib E, Bakhtiari S, and Hurmuzlu Y (2021) Real time control of tethered satellite systems to de-orbit space debris. Aerospace Science Technology. 109: 106379. https://doi.org/10.1016/j.ast.2020.106379.

Svotina V, and Cherkasova M (2023) Space debris removal–review of technologies and techniques. Flexible or virtual connection between space debris and service spacecraft. Acta Astronautica. 204: 840-853. https://doi.org/10.1016/j.actaastro.2022.09.027.

Modi V, Lakshmanan P, and Misra A (1990) Dynamics and control of tethered spacecraft-a brief overview. Paper presented at the Dynamics Specialists Conference. https://doi.org/10.2514/6.1990-1195.

Kumar K (2006) Review on dynamics and control of nonelectrodynamic tethered satellite systems. Journal of Spacecraft and Rockets. 43: 705-720. https://doi.org/10.2514/1.5479.

Sanmartin JR, Lorenzini EC, and Martinez-Sanchez M (2010) Electrodynamic tether applications and constraints. Journal of Spacecraft and Rockets. 47: 442-456. https://doi.org/10.2514/1.45352.

Huang P, Zhang F, Chen L, Meng Z, Zhang Y, Liu Z, and Hu Y (2018) A review of space tether in new applications. Nonlinear Dynamics. 94: 1-19. https://doi.org/10.1007/s11071-018-4389-5.

Sánchez-Arriaga G, Lorenzini EC, and Bilén SG (2024) A review of electrodynamic tether missions: Historical trend, dimensionless parameters, and opportunities opening space markets. Acta Astronautica. https://doi.org/10.1016/j.actaastro.2024.09.002.

Zheng P, Cao X, and Zhang S (2008) J2 perturbation effect on the deployment of tether-assisted deorbit system. Paper presented at the 2008 2nd International Symposium on Systems and Control in Aerospace and Astronautics. https://doi.org/10.1109/ISSCAA.2008.4776269.

Yu B, and Jin D (2010) Deployment and retrieval of tethered satellite system under J2 perturbation and heating effect. Acta Astronautica. 67: 845-853. https://doi.org/10.1016/j.actaastro.2010.05.013.

Yu B, Jin D, and Wen H (2016) Nonlinear dynamics of flexible tethered satellite system subject to space environment. Applied Mathematics and Mechanics. 37: 485-500. https://doi.org/10.1007/s10483-016-2049-9.

Yu B, Xu S, and Jin D (2020) Chaos in a tethered satellite system induced by atmospheric drag and earth's oblateness. Nonlinear Dynamics. 101: 1233-1244. https://doi.org/10.1007/s11071-020-05844-8.

Yuan W, Deng H, and Liu J (2024) Chaotic libration and control of a space tether-sail system in earth polar orbits with J2 perturbation. Applied Mathematical Modelling. 136: 115617. https://doi.org/10.1016/j.apm.2024.07.024.

Hallaj MaA, and Assadian N (2016) Sliding mode control of electromagnetic tethered satellite formation. Advances in Space Research. 58: 619-634. http://dx.doi.org/10.1016/j.asr.2016.05.019.

Tikhonov A, Antipov K, Korytnikov D, and Nikitin DY (2017) Electrodynamical compensation of

disturbing torque and attitude stabilization of a satellite in J2 perturbed orbit. Acta Astronautica. 141: 219-227. https://doi.org/10.1016/j.actaastro.2017.10.009.

Razzaghi P, Al Khatib E, and Bakhtiari S (2019) Sliding mode and sdre control laws on a tethered satellite system to de-orbit space debris. Advances in Space Research. 64: 18-27. https://doi.org/10.1016/j.asr.2019.03.024.

Liu J, Zhu ZH, Li G, and Zhan X (2021) Fuzzy-based continuous current control of electrodynamic tethers for stable and efficient orbital boost. Aerospace Science Technology. 118: 106999. https://doi.org/10.1016/j.ast.2021.106999.

Aslanov V, and Ledkov A. (2012). Dynamics of tethered satellite systems: Elsevier.

Stevens RE. (2008). Optimal control of electrodynamic tether satellites. (Ph.D. Ph.D.), Air Force Institute of Technology,

Kéchichian JA. (2021). Orbital relative motion and terminal rendezvous: Springer.

Zhong R, and Zhu Z (2013) Libration dynamics and stability of electrodynamic tethers in satellite deorbit. Celestial Mechanics and Dynamical Astronomy. 116: 279-298. https://doi.org/10.1007/s10569-013-9489-4.

Aslanov VS (2024) Suppressing chaotic oscillations of a tether anchored to the phobos surface under the l1 libration point. Chaos, Solitons and Fractals. 181: 114663. https://doi.org/10.1016/j.chaos.2024.114663.

Liu J. (2017). Sliding mode control using matlab: Academic Press.

الملخص العربي

عنوان البحث: قمع الفوضى في نظام قمر صناعي كهروديناميكي مربوط باستخدام التحكم بأسلوب الانزلاق تحت تأثير اضطراب معامل J_2

أحمد يوسف*[١]، أحمد مجدي عبد العزيز[٢]، عبد الحكيم أبو الفتوح عبد النبي[١]، يحيى أحمد عبد العزيز

[١]قسم الرياضيات، كلية العلوم، جامعة دمياط، دمياط، مصر.
[٢] المركز القومي لبحوث الفلك والجيوفيزياء (NRIAG)، القاهرة، مصر.

يتناول هذا البحث دراسة السلوك الفوضوي لنظام قمر صناعي كهروديناميكي مربوط يتحرك داخل مستوٍ مداري دائري حول الأرض تحت تأثير تفلطح الأرض المُمثل بمعامل J_2.
تم نمذجة النظام باستخدام نموذج الدمبل، حيث تم اشتقاق معادلات الحركة باستخدام منهج لاغرانج مع أخذ تأثير كل من القوة الكهرومغناطيسية الناتجة عن تفاعل التيار المار في الحبل مع المجال المغناطيسي الأرضي، بالإضافة إلى تأثير التفلطح الأرضي في الحسبان.
تم استخدام تحليل ميلنيكوف لاشتقاق شرط ضروري لظهور السلوك الفوضوي في النظام. ولمعالجة هذه الفوضى، تم اقتراح استراتيجية تحكم جديدة تعتمد على التحكم بأسلوب الانزلاق(SMC) ، حيث يُستخدم طول الحبل كإشارة تحكم. يهدف المتحكم إلى كبح السلوك الفوضوي وتوجيه النظام إما نحو حالة تذبذب منتظمة أو نحو نقطة توازن محددة مسبقًا.
أُجريت محاكاة عددية للتحقق من صحة الشروط التحليلية ولتقييم فعالية المتحكم المقترح. أظهرت النتائج قدرة المتحكم على تثبيت النظام والقضاء على السلوك الفوضوي غير المرغوب فيه، مما يدل على قوة وفعالية الطريقة المقترحة. ومع ذلك، توصي الدراسة بإجراء تجارب عملية مستقبلًا للتحقق من فعالية هذا المتحكم على أرض الواقع. وتُعد هذه الدراسة مساهمة مهمة في فهم ديناميكا أنظمة الأقمار الصناعية المربوطة وتطوير طرق تحكم موثوقة لتطبيقات الفضاء الفعلية.